Eur. Phys. J. D (2016) 70: 185
DOI: 10.1140/epjd/e2016-60662-3

THE EUROPEAN PHYSICAL JOURNAL D

Regular Article

Slow light enhanced atomic frequency comb quantum memories in photonic crystal waveguides*

Chenzhi Yuan[a], Wei Zhang, Yidong Huang, and Jiangde Peng

Tsinghua National Laboratory for Information Science and Technology, Department of Electronic Engineering, Tsinghua University, Beijing 100084, P.R. China

Received 22 November 2015 / Received in final form 14 May 2016
Published online 8 September 2016 –

Abstract. In this paper, we propose a slow light-enhanced quantum memory with high efficiency based on atomic frequency comb (AFC) in ion-doped photonic crystal waveguide (PCW). The performance of the quantum memory is investigated theoretically, considering the impact of the signal bandwidth. Both the forward and backward retrieval schemes are analyzed. In the forward retrieval scheme, the analysis shows that a moderate slow light effect can improve the retrieval efficiency to above 50% with very high fidelity, even when the intrinsic optical depth is very low and the signal bandwidth is comparable with the AFC bandwidth. In the backward retrieval scheme, retrieval efficiency larger than 90% can be obtained and fidelity can remain above 90% for signal with bandwidth much narrower than AFC bandwidth, when moderate slow light is introduced into waveguide with low intrinsic optical depth. Although the phase mismatching effect limits the slow light enhancement on retrieval efficiency and decreases the fidelity for signal with bandwidth approaching AFC bandwidth, we design a modified atomic frequency comb structure (MAFC) based on which a moderate slow light can make the retrieval efficiency larger than 85% and keep the fidelity above 80%. Our calculations show that the proposed scheme provides a promising way to realize high efficiency on-chip quantum memory.

1 Introduction

Quantum memory is a crucial element for future quantum networks [1], as a basic function utilized in quantum repeaters [2,3], deterministic single-photon sources [4], measurement-device-independent quantum key distribution [5] and so on. Several approaches have been proposed to realize quantum memory, including electromagnetically induced transparency (EIT) [6,7], off-resonant Raman interactions [8,9], and schemes employing photon echo protocols, such as controlled reversible inhomogeneous broadening (CRIB) [10,11], gradient echo memory (GEM) [12], revival of silenced echo (ROSE) [13,14], and atomic frequency comb (AFC) [15,16]. Compared with other approaches, the approach based on AFC has the ability to store temporal multimode signals independent of optical absorption depth, hence, it attracted much attention in recent years.

The storages of photons at telecom wavelengths [17], energy-time entangled photon pairs [18], photon qubits in polarization [19,20], and hyper-entangled photon pairs [21] have been demonstrated via the AFC-based protocol. To achieve sufficiently broad inhomogeneous broadening, all the experimental implementations of quantum memory based on AFC are in rare-earth ion doped crystals or glass, such as Pr^{3+}:Y_2SiO_5 [22,23], Nd^{3+}:Y_2SiO_5 [16], Nd^{3+}:YVO_4 [18], and Er^{3+}-doped fibers [17]. However, It is difficult to realize an high optical depth in the rare-earth ion doped crystal, since the concentration of ions doped in the crystal is usually limited to reduce the decoherence induced by the strong interaction between the adjacent ions. The creation of AFC further reduce the optical depth. Therefore, compared with quantum memory based on other protocols which can be implemented in atomic gases [24,25], the efficiency of the AFC-based method are still limited. For bright light, the highest storage efficiency is 35% [26], and the storage efficiency for the signal at single photon level is usually lower than 10% [16–19,22]. This shortcoming gets much severe when on chip quantum memory of small size is developed [27,28]. Recently, it has been proposed and demonstrated that the efficiency of the quantum memory based on AFC can be improved significantly by placing the rare earth doped crystal into an optical cavity [29–31]. The experiment shows that the retrieval efficiency increases from 1% to 56% thanks to the effect of the cavity [31]. However, this approach has some disadvantages if on-chip realization is considered.

* Supplementary material in the form of one pdf file available from the Journal web page at
http://dx.doi.org/10.1140/epjd/e2016-60662-3

[a] e-mail: ycz13@mails.tsinghua.edu.cn

The complicated interaction between the AFC and cavity mode [31,32] makes the cavity design and AFC measurement challenging, and the inevitable unexpected loss in micro or nanocavity lowers the storage and retrieval efficiency significantly.

In this paper, we propose a slow light-enhanced quantum memory scheme based on AFC in rare-earth doped photonic crystal waveguide (PCW). Both the forward and backward retrieval schemes are analyzed theoretically, with the consideration of the signal bandwidth. In the forward retrieval scheme, under a moderate slow light effect with a group index $n_g = 37$, the theoretical analysis shows that the retrieval efficiency can be improved from about 1% to above 50% in a system with very low intrinsic optical depth, even when the signal bandwidth is comparable with AFC bandwidth. Though the slowing light also enhances the AFC induced dispersion and intensifies the fidelity degrade with increasing signal bandwidth, slow light effect with $n_g = 37$ can still keep the fidelity above 90% for signal with bandwidth approaching AFC bandwidth. In the backward retrieval scheme, the theoretical analysis shows that a moderate slow light effect in PCW with low optical depth can improve the retrieval efficiency to above 90% for signal with bandwidth much narrower than AFC bandwidth, while keeps the fidelity above 90%. Though the phase mismatching effect in the backward retrieval scheme limits the slow light enhancement on retrieval efficiency and reduces the fidelity for signal with bandwidth approaching AFC bandwidth, our calculation shows that retrieval efficiency and fidelity, higher than 85% and 80%, respectively, can be simultaneously achieved in PCW with moderate slow light effect, by introducing a modified atomic frequency comb structure (MAFC), designed according to the principle in reference [33].

2 Scheme description

A sketch of the AFC-based quantum memories in waveguides is shown in Figure 1. Atoms or ions are doped into the waveguide as an ensemble. The absorption of signal in the ensemble is due to the transitions from the ground state $|g\rangle$ to the excited state $|e\rangle$ of the atoms or ions, each of which is homogeneously broadened. An absorption comb, namely the AFC, can be realized by a train of elaborate pump pulses [28]. These pump pulses burn a broad hole on the absorption spectrum, while the periodical comb-like peaks are left in the hole, as shown in the absorption spectrum in Figure 1a. As a type of quantum memory utilizing the photon echo technology [10,34–36], the storage and retrieval processes of the AFC-based protocols can be implemented in two configurations depending on whether on-demand retrieval is required, which are shown in Figures 1b and 1c, respectively. In the scheme shown in Figure 1b, when the signal pulse is injected and travels through the waveguide shown in Figure 1b.1, a fraction of the photons in the pulse would be absorbed and mapped into the collective excitation state in the AFC, i.e., be stored. After a duration in which the dephasing and rephasing processes occur successively, the

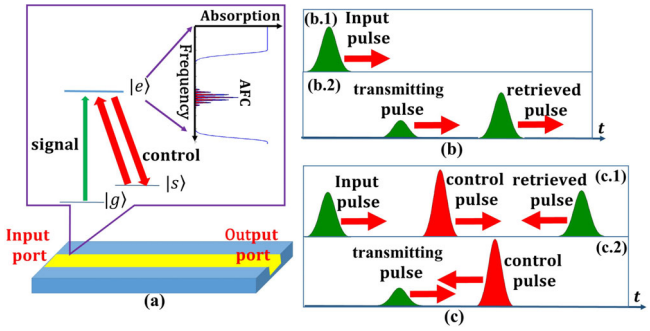

Fig. 1. The sketch of AFC-based quantum memory the in waveguide. (a) The illustration and port definition of the waveguide. The inset shows the energy levels of the atoms and profile of AFC. For simplicity, in the illustration the creation of the AFC is attributed to the engineering of the excited states. (b) The pulse sequence in the input port (b.1) and output port (b.2) in the forward retrieval scheme. (c) The pulse sequence in the input port (c.1) and output port (c.2) in the backward retrieval scheme.

photons will be mapped out and retrieved forward from the output port of the waveguide, as shown in Figure 1b.2. In the scheme shown in Figure 1c, after the input signal is stored, two counter-propagating control light pulses are successively injected into and travel through the waveguide as shown in Figures 1c.1 and 1c.2. The first control light pulse transfers the optical coherence between $|g\rangle$ and $|e\rangle$ to spin coherence between $|g\rangle$ and another ground state $|s\rangle$ shown in Figure 1a. The second one realizes the reverse process of the above transfer and achieves the function of on-demand retrieval. The retrieved photons travel backwardly and output from the input port of the waveguide. For simplicity, these two schemes will be called forward and backward retrieval schemes, respectively, in the following descriptions. In both schemes, a fraction of photons in the signal pulse would travel through the waveguide directly without interacting with the AFC, forming the transmitting pulse, which is also shown in Figures 1b.2 and 1c.2.

Due to the limited concentration of the doped ions, high intrinsic optical depth is difficult to be realized in the doped waveguide. It can be expected that most input signal photons would travel through the waveguide without interacting with the AFC, leading to strong transmitting pulses and weak retrieved pulses. Hence, the storage efficiency of the memory is limited by the low intrinsic optical depth of the waveguide. Recently, photonic crystal waveguide (PCW) structures with strong slow light effects have been developed [37–40]. In PCW, the group velocity of the waveguide mode is highly reduced due to the multi-scattering processes in the periodical structure. Here we introduce the PCW with slow light into the schemes of quantum memory based on the AFC. For the slow light mode in PCW, the temporally compression effect enhances the electrical field intensity of the light significantly, hence, provides large coupling strength between the light and doped atomic ensemble, which will increase the optical depth. On one hand, such enhancement improves the performance of the storage process

by enhancing the coherent absorption of the signal photons into AFC. On the other hand, it enhances the reemission process and makes the retrieving process more efficiently. In the following sections, we will investigate the effect of slow light on the performance of AFC-based quantum memory in waveguides theoretically.

3 Absorption of AFC in PCW with slow light

Considering that a light pulse is traveling forward along a PCW with a length of L, the positive frequency component operator of the light field can be expressed as

$$E_f^+(z,t) = i\sqrt{\frac{\hbar\omega_0}{4\pi\varepsilon_0 v_g A}}\int d\omega \hat{a}_f(z,\omega)\, e^{-i(\omega t-\frac{\omega_0 z}{v_p})}, \quad (1)$$

where ω_0 is the central angular frequency of the pulsed light; A is the effective modal area of the guiding mode in the PCW; v_p and v_g are the phase and group velocities of the slow light mode at the frequency of the signal light, respectively [41]. For different n_g, A is treated as constant to simplify the calculation. This assumption is reasonable since the PCWs realizing different n_g at the same wavelength should be designed respectively, by which their modal fields could be optimized to be the same. For slow light mode in PCW, the group velocity v_g is far smaller than the light speed in bulk dielectric materials. Hence, the expression shows that the light field of the waveguide mode can be highly enhanced by the slow light effect, since its amplitude is in inverse proportion to the v_g. In the expression, the uniform transverse light distribution is used for simplicity. The results under this assumption could be modified to the case with a complex transverse field distribution if the overlapping integration between the light field and the transverse distribution of the doped ions is considered. The v_p and v_g are treated as two constant parameters of the waveguide mode under the condition that the signal bandwidth is narrow relative to the central frequency. Utilizing the annihilation operator $\hat{a}_f(z,\omega)$, the photon flux amplitude operator can be defined as $\hat{a}_f(z,t) = \int d\omega \hat{a}_f(z,\omega)\, e^{-i(\omega-\omega_0)t}/\sqrt{2\pi}$, where the rapidly varying term of $e^{-i\omega_0(t-z/v_p)}$ are dropped for simplicity. The forward photon flux can be obtained by $I_f(z,t) = \langle a_f^\dagger(z,t)\hat{a}_f(z,t)\rangle$. For the light pulses travelling backward in the waveguide, the electrical field operator $E_b^+(z,t)$, the photon flux amplitude operator $\hat{a}_b(z,t)$ and the photon flux $I_b(z,t)$ can be defined in the same way.

For an atom doped in the waveguide, the atomic coherence operators can be expressed as

$$\begin{aligned}
\hat{\sigma}^{ge}(z,t;\omega_{ge}) &= |g,z,\omega_{ge}\rangle\langle e,z,\omega_{ge}|,\\
\hat{\sigma}^{eg}(z,t;\omega_{ge}) &= |e,z,\omega_{ge}\rangle\langle g,z,\omega_{ge}|,\\
\hat{\sigma}^{gg}(z,t;\omega_{ge}) &= |g,z,\omega_{ge}\rangle\langle g,z,\omega_{ge}|,\\
\hat{\sigma}^{ee}(z,t;\omega_{ge}) &= |e,z,\omega_{ge}\rangle\langle e,z,\omega_{ge}|
\end{aligned}$$

and

$$\hat{\sigma}^z(z,t;\omega_{ge}) = \hat{\sigma}^{ee}(z,t;\omega_{ge}) - \hat{\sigma}^{gg}(z,t;\omega_{ge}),$$

where $|g,z,\omega_{ge}\rangle$ and $|e,z,\omega_{ge}\rangle$ are the ground state and excited state of the atom at the location z, respectively. ω_{ge} is the resonant frequency of the transition from the ground to the excited states. In the ensemble, the transition has a frequency distribution, which can be described by a normalized distribution function $n(\omega_{ge})$. In the representation with the bases of $|e,z,\omega_{ge}\rangle$ and $|g,z,\omega_{ge}\rangle$, the intrinsic Hamiltonian of the atoms in the waveguide can be expressed as

$$\hat{H}_0 = \hbar N_0 \int d\omega_{ge} n(\omega_{ge}) \int dz' \hat{\sigma}^{ee}(z',t;\omega_{ge})/L,$$

where N_0/L is the line density of the atoms along the waveguide. The Hamiltonian describing the interaction between the atoms and the forward (backward) propagating light field can be written as

$$\begin{aligned}
\hat{H}_{I,f(b)} = -i\sqrt{2\pi}\hbar\mu_{eg}\kappa N_0 &\int d\omega_{ge} n(\omega_{ge})\\
&\times \int dz' \hat{a}_{f(b)}(z',t)\,\hat{\sigma}^{eg}(z',t;\omega_{ge})\\
&\times e^{-i\omega_0(t-z/v_p)}/L + \text{H.c},
\end{aligned}$$

where $\kappa = \sqrt{\omega_0/4\pi\hbar\varepsilon_0 v_g A}$ and μ_{eg} is the dipole momentum of the transition between ground and excited states [42]. In the following calculations, we use $\hat{\sigma}_f^{ge}(z,t;\omega_{ge})$ and $\hat{\sigma}_f^z(z,t;\omega_{ge})$ to represent the slowly varying envelope of the forward propagating pseudo-spin wave, and those of the backward propagating pseudo-spin wave is represented by $\sigma_b^{ge}(z,t;\omega_{ge})$ and $\sigma_b^z(z,t;\omega_{ge})$, respectively. Here, the terms of the forward and backward rapidly varying carriers $e^{-i\omega_0(t-z/v_p)}$ and $e^{-i\omega_0(t+z/v_p)}$ are dropped, respectively.

Substituting $\hat{H}_{I,f}$ and $\hat{\sigma}_f^{ge}(z,t)$ into the Heisenberg equation, we can get

$$\begin{aligned}
\dot{\hat{\sigma}}_f^{ge}(z,t;\Omega) = &-i\Omega\hat{\sigma}_f^{ge}(z,t;\Omega)\\
&+\sqrt{2\pi}\kappa\mu_{eg}\hat{\sigma}_f^z(z,t;\Omega)\,\hat{a}_f(z,t), \quad (2)
\end{aligned}$$

where $\Omega = \omega_{ge} - \omega_0$ is the detuning between ω_{ge} and ω_0. The commutation relation

$$\begin{aligned}
[\hat{\sigma}^{ge}(z,t;\Omega), \hat{\sigma}^{ge}(z',t;\Omega')] = &-\delta(z-z',\Omega-\Omega')\\
&\times \hat{\sigma}^z(z,t;\Omega)\,[N_0 n(\Omega)/L]^{-1}
\end{aligned}$$

is utilized in the derivation of equation (2). When a light pulse propagates along the PCW, the operator $\hat{a}_f(z,t)$ satisfies

$$\begin{aligned}
\left(\frac{\partial}{\partial z} + \frac{1}{v_g}\frac{\partial}{\partial t}\right)\hat{a}_f(z,t) = &\sqrt{2\pi}\kappa\mu_{eg}\kappa N_0\\
&\times \int \frac{d\Omega n(\Omega)\,\hat{\sigma}_f^{ge}(z,t;\Omega)}{L}, \quad (3)
\end{aligned}$$

where $n(\Omega)$ in the right hand side (RHS) of equation (3) is another form of $n(\omega_{ge})$ under $\Omega = \omega_{ge} - \omega_0$ [42]. For simplicity, we suppose a Gaussian AFC structure

$$n(\Omega) = r_a n_a e^{-\Omega^2/2\Gamma^2} \sum_{n=-\infty}^{\infty} e^{-(\Omega-n\Delta)^2/2\gamma_a^2}, \quad (4)$$

where $\Gamma/2\pi$ is the comb envelope width; $\gamma_a/2\pi$ is the peak width, and $\Delta/2\pi$ is the space between two adjacent peaks, respectively. The coefficient r_a is defined by $r_a = \gamma_a/\Delta$. It represents the ratio of the atoms which could interact with the light field in the AFC bandwidth. Moreover, $n(\Omega)$ is normalized by $\int d\Omega n(\Omega) = r_a$ and n_a is the factor for the normalization.

The solution of equation (3) can be calculated under the conditions that (i) the input light pulses are weak, and (ii) the temporal width of the input pulses is much smaller than $2\pi/\Delta$. The details of the derivation are shown in Appendix A of the Supplementary material and a solution in the time range of $t \ll 2\pi/\Delta$, defined as $\hat{a}_f^{(0)}(z,t)$, is shown in equation (5),

$$\hat{a}_f^{(0)}(z,t) = \frac{1}{2\pi}\int d\Omega e^{i\left(\Omega t - \frac{\Omega z}{v_g} + \frac{\alpha_0 n_g n_1(\Omega) z}{2}\right)} \times e^{-\frac{\alpha_0 n_g n_0(\Omega) z}{2}} \hat{a}_f^{in}(0,\Omega), \quad (5)$$

where

$$n_0(\Omega) = e^{-\Omega^2/2\Gamma^2}$$

and

$$n_1(\Omega) = e^{-\Omega^2/2\Gamma^2}\mathrm{erfi}(-\Omega/\sqrt{2}\Gamma);$$

$$\alpha_0 = 2\pi\omega_0\mu_{eg}^2 N_0 r_a^2/\Gamma\hbar\varepsilon_0 cLA$$

is the intrinsic absorption coefficient of the AFC in waveguide; $n_g = c/v_g$ is the group index of the waveguide mode; $\hat{a}_f^{in}(0,\Omega)$ is the Fourier transformation of the photon flux amplitude of the input signal field. The term $e^{i\alpha_0 n_g n_1(\Omega) z/2}$ and $e^{-\alpha_0 n_g n_0(\Omega) z/2}$ presents the AFC induced dispersion and absorption, respectively. This equation reveals that the photon flux amplitude $\hat{a}_f(z,t)$ in the waveguide can be represented by a transformation of the input amplitude $\hat{a}_f^{in}(0,t)$. Then, the photon flux of the transmitting pulses at the output port of the waveguide can be calculated as

$$\begin{aligned} I_f^{(0)}(z,t) &= \langle \hat{a}_f^{(0)\dagger}(z,t)\hat{a}_f^{(0)}(z,t)\rangle \\ &= \left(\frac{1}{2\pi}\right)^2 \int d\Omega_1 \\ &\quad \times \int d\Omega_2 e^{i\left[(\Omega_2-\Omega_1)\left(t-\frac{z}{v_g}\right)+\frac{\alpha_0 n_g (n_1(\Omega_2)-n_1(\Omega_1))z}{2}\right]} \\ &\quad \times e^{-\frac{\alpha_0 n_g L}{2}[n_0(\Omega_1)+n_0(\Omega_2)]} \\ &\quad \times \int dt_1 \int dt_2 e^{i(\Omega_1 t_1 - \Omega_2 t_2)} G_f^{(0)}(0,t_1,t_2), \end{aligned} \quad (6)$$

where $G_f^{(0)}(0,t_1,t_2)$ is the autocorrelation function of the input pulse at $z = 0$. Compared with the photon flux of the input pulse,

$$I_f^{in}(0,t) = \left(\frac{1}{2\pi}\right)^2 \int d\Omega_1 \int d\Omega_2 e^{i(\Omega_2-\Omega_1)t} \times \int dt_1 \int dt_2 e^{i(\Omega_1 t_1 - \Omega_2 t_2)} G_f^{in}(0,t_1,t_2), \quad (7)$$

$I_f^{(0)}(z,t)$ in equation (6) is attenuated by a factor of $e^{-\alpha n_g z[n_0(\Omega_1)+n_0(\Omega_2)]/2}$ for every combination of frequencies components Ω_1 and Ω_2 in the integral. This factor decreases exponentially with increasing n_g, showing that the transmitting pulse is reduced significantly if slow light effect is introduced.

If the input light has a Gaussian profile in time domain, the photon flux of the transmitting pulses can be calculated explicitly. The detail of the calculation is shown in Appendix C of the Supplementary material. It shows that if the input light is a single Gaussian pulse with a photon flux amplitude of $a(t) = \sqrt{I_0}e^{-(\gamma_s t)^2/2}$, the photon flux of the transmitting pulses is

$$I_f^{(0)}(L,t) = \left(\frac{1}{2\pi}\right)^2 \left| \int d\Omega e^{i\left(\Omega t - \frac{\Omega L}{v_g} + \frac{\alpha_0 n_g L n_1(\Omega)}{2}\right)} \times e^{-\frac{\alpha_0 n_g L n_0(\Omega)}{2}} a(\Omega) \right|^2, \quad (8)$$

where $a(\Omega)$ is the Fourier transformation of $a(t)$. If the input light is a train of Gaussian pulses with photon flux amplitudes of $a_j(t) = e^{-[\gamma_s(t-t_{0j})]^2/2}$ $(j = 1,\ldots,N)$, namely, temporal multimode Gaussian pulses, the photon flux of the transmitting pulses is

$$I_f^{(0)}(L,t) = \left(\frac{1}{2\pi}\right)^2 \sum_{j=1}^{N} \left| \int d\Omega e^{i\Omega\left(t-\frac{L}{v_g}-t_{0j}+\frac{\alpha_0 n_g L n_1(\Omega)}{2}\right)} \times e^{-\frac{\alpha_0 n_g L n_0(\Omega)}{2}} a(\Omega) \right|^2. \quad (9)$$

From equations (7) and (9), we can see that the absorption of all the input pulses can be enhanced by slow light. Furthermore, we can define transmitting ratio R_e to characterize the transmitting probability for the input photons, which can be expressed as

$$R_t = \int_{\tau_d+t_1}^{\tau_d+t_2} I_f^{(0)}(L,t)\,dt \Big/ \int_{t_1}^{t_2} I_f^{in}(0,t)dt, \quad (10)$$

with $t_2 = t_{0N} + 2\pi/\gamma_s$ and $t_1 = -2\pi/\gamma_s$, i.e., the ratio of the area under the transmitting pulses to that under the input pulses. Here, the center of the first pulse in the input train of pulses is defined as $t_{01} = 0$. The term $2\pi/\gamma_s$ is the temporal width of the Gaussian pulse and τ_d is the transiting time of the pulse in the PCW.

In Figure 2, the transmitting ratio R_t for a single Gaussian pulse in the waveguide with an intrinsic optical depth of $\alpha_0 L = 0.05$ and a length of $L = 100$ μm is calculated and plotted under increasing n_g. Using such short length, the propagation loss of PCW is low, and most of the photons coupling into the PCW will participate in the storage and retrieval processes. The calculations are based on equation (8). The AFC used in the calculation has a bandwidth of $\Gamma/2\pi = 8$ MHz, a peak-peak spacing of $\Delta/2\pi = 1$ MHz and a single peak width of $\gamma_a/2\pi = 0.1$ MHz, the magnitude orders of which are

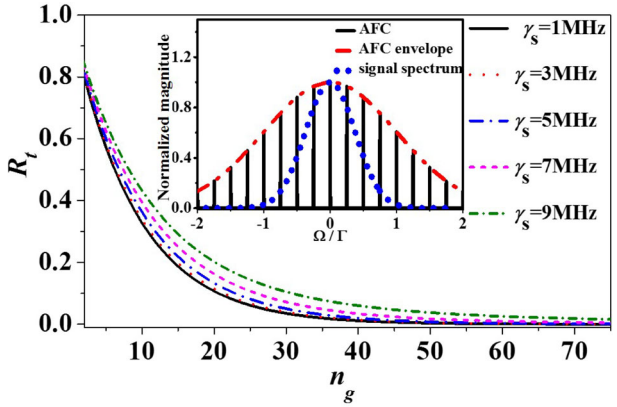

Fig. 2. The transmitting ratio R_t when a single Gaussian pulse with bandwidth of $\gamma_s/2\pi = 1$ MHz (black solid line), 3 MHz (red dotted), 5 MHz (blue dash dotted), 7 MHz (pink dashed) and 9 MHz (green short dashed dot) is input into a waveguide with intrinsic optical depth of $\alpha L = 0.05$ and length of $L = 100$ μm. The horizontal coordinate is the group index n_g of the slow light mode. The AFC in PCW has bandwidth of $\Gamma/2\pi = 8$ MHz, peak-peak spacing $\Delta/2\pi = 1$ MHz and single peak width $\gamma_a/2\pi = 0.1$ MHz. In the inset, the black solid line shows the normalized absorption spectrum of the AFC. The red dashed line shows its envelope, and the blue dotted line presents the normalized spectrum of the input signal with $\gamma_s/2\pi = 3$ MHz.

referred to the experiments of quantum memory based on the AFC in praseodymium-doped crystals [22]. We can see that R_t shows exponential-like decrease with increasing n_g, which means that the transmitting probability for the input photons decreases sharply if the slow light effect is introduced. On the other hand, R_e increases slightly with rising γ_s. It can be intuitively explained by equation (8), in which the attenuation is expressed with a factor of $e^{-\alpha_0 n_g n_0(\Omega)L/2}$, showing that the attenuation get weaker under higher frequency component Ω. It can be seen that even though the signal bandwidth increases to $\gamma_s/2\pi = 7$ MHz, which is near the AFC bandwidth $\Gamma/2\pi$, R_e can be controlled to be lower than 5% with a moderate n_g of 37. This result shows that the slow light effect in PCW can significantly enhance the absorption process in AFC-based quantum memory.

4 Retrieval processes of the AFC-based quantum memory in PCW with slow light

4.1 The forward retrieval scheme

In the forward retrieval scheme, the retrieved light pulses output at $z = L$. If the input signal pulses are injected into the waveguide at $t = 0$, the transmitting pulses will leave the waveguide around $t_e = 2\pi/\gamma_s + \tau_d$, and the retrieved pulse will leave the waveguide at $t_r \approx 2\pi/\gamma_s + 2\pi/\Delta$. Here, $2\pi/\Delta$ is the storage time of the light pulses in the waveguide, which is determined by the space Δ between the two adjacent peaks in the AFC. Considering a specific time T_0 satisfying $t_e \ll T_0 \ll t_r$, the solution of equation (2) at $t = T_0$ is

$$\hat{\sigma}_f^{ge}(z, T_0; \Omega) = \sqrt{2\pi}\kappa\mu_{eg} \int_{-\infty}^{T_0} dt' e^{-i\Omega(T_0 - t')} \hat{a}_f(z, t'). \tag{11}$$

The evolution of $\hat{\sigma}_f^{ge}(z, t; \Omega)$ after $t = T_0$ can be expressed as

$$\hat{\sigma}_f^{ge}(z, t; \Omega) = \hat{\sigma}_f^{ge}(z, T_0; \Omega) e^{-i\Omega(t - T_0)} + \sqrt{2\pi}\kappa\mu_{eg} \int_{T_0}^{t} dt'' e^{-i\Omega\left(t - t''\right)} \hat{a}_f\left(z, t''\right). \tag{12}$$

Substituting equation (12) into equation (3), we can obtain

$$\left(\frac{\partial}{\partial z} + \frac{1}{v_g}\frac{\partial}{\partial t}\right)\hat{a}_f(z, t) = -\frac{\alpha_0 n_g}{2\pi} \times \left[\int_{-\infty}^{T_0} dt' \tilde{n}(t - t')\hat{a}_f(z, t') + \int_{T_0}^{t} dt'' \tilde{n}(t - t'')\hat{a}_f(z, t'')\right], \tag{13}$$

where $\tilde{n}(t)$ is the inverse Fourier transformation of the distribution $n(\Omega)$ in equation (4). Under the assumption that the temporal width of the pulse is far smaller than the storage time, i.e. $2\pi/\gamma_s \ll 2\pi/\Delta$, a frequency domain solution of equation (13) can be obtained as

$$\left(\frac{\partial}{\partial z} + \frac{i\Omega}{v_g}\frac{\partial}{\partial t}\right)\hat{a}_f^{(1)}(z, \Omega) = -\frac{\alpha_0 n_g}{2} e^{-\frac{\gamma_a^2}{2}\left(\frac{2\pi}{\Delta}\right)^2} \times e^{-\frac{i\Omega 2\pi}{\Delta}} \hat{a}_f^{(0)}(z, \Omega) + \frac{\alpha_0 n_g}{2}\left(n_0(\Omega) + i n_1(\Omega)\right) \times \hat{a}_f^{(1)}(z, \Omega), \tag{14}$$

where $\hat{a}_f^{(1)}(z, \Omega)$ is frequency domain presentation of $\hat{a}_f^{(1)}(z, t)$, the photon flux amplitude operator of the first retrieved pulse after T_0; the term $e^{-(2\pi\gamma_a/\Delta)^2/2}$ describes the decay of the collective excitation of the atoms in the AFC due to the decoherence during the storage process. The first term on the RHS of equation (14) is related to $\hat{a}_f^{(0)}(z, \Omega)$, and is a transformation of $\hat{a}_f(0, t)$ according to equation (5). So it describes the generation process of the reemitted light when the polarizations of the atoms are rephasing. The second term on the RHS of equation (14) describes the reabsorption process in the propagation of the reemitted light, since it presents the polarization induced by $\hat{a}_f^{(1)}(0, t)$ itself.

The photon flux amplitude of the retrieved pulsed light at $z = L$ can be calculated by solving equation (14) and the result is

$$\hat{a}_f^{(1)}(L,t) = -\frac{\alpha_0 n_g L}{2\pi} e^{-\frac{\gamma_a^2}{2}\left(\frac{2\pi}{\Delta}\right)^2} \times \int d\Omega e^{i\left(\Omega t - \frac{\Omega L}{v_g} + \frac{\alpha_0 n_g L n_1(\Omega)}{2}\right)} \times e^{-\frac{\alpha_0 n_g L n_0(\Omega)}{2}} n_0(\Omega)\, \hat{a}_f^{in}(0,\Omega). \quad (15)$$

The derivation process of this equation can be seen in Appendix B of the Supplementary material. It is obvious that in equation (15) the retrieved photon flux amplitude is expressed as a transformation of that of the input light.

If the input signal light is a single Gaussian pulse with a photon flux amplitude of $a(t) = \sqrt{I_0} e^{-(\gamma_s t)^2/2}$, substituting equation (15) into $I_f^{(1)}(L,t) = \langle a_f^{(1)\dagger}(z,t) a_f^{(1)}(z,t)\rangle$, the photon flux of the retrieved light pulse can be calculated by the process shown in Appendix C of the Supplementary material, and the result is

$$I_f^{(1)}(L,t) = \left(\frac{1}{2\pi}\right)^2 (\alpha_0 n_g L)^2 e^{-\left(\frac{2\pi\gamma_a}{\Delta}\right)^2} \times \left| \int d\Omega e^{i\left[\Omega\left(t - \frac{2\pi}{\Delta} - \frac{L}{v_g}\right) + \frac{\alpha_0 n_g L n_1(\Omega)}{2}\right]} \times e^{-\frac{\alpha_0 n_g L n_0(\Omega)}{2}} n_0(\Omega)\, a(\Omega) \right|^2, \quad (16)$$

where $a(\Omega)$ is the Fourier transformation of $a(t)$ and $\Gamma/2\pi$ is the envelope width of the AFC. It is obvious that the retrieved pulse has a time delay of $2\pi/\Delta$, besides L/v_g and the delay brought by the AFC induced dispersion. This time delay indicates that the storage of the signal light pulse is achieved.

We can define the retrieval efficiency as

$$\eta_r = \frac{\int_{2\pi/\Delta+\tau_d+t_1}^{2\pi/\Delta+\tau_d+t_2} I_f^{(1)}(L,t)dt}{e^{-\left(\frac{2\pi\gamma_a}{\Delta}\right)^2} \int_{t_1}^{t_2} I_f^{in}(0,t)\, dt},$$

where $e^{-(2\pi\gamma_a/\Delta)^2}$ in the denominator is used to exclude the signal dissipation due to decoherence effect, and t_1, t_2 and τ_d have been defined in the definition of the transmitting ratio R_t in Section 3. The expression of η_r can be seen in Appendix D of the Supplementary material and the analysis there also shows that the dependences of η_r on n_g and γ_s can be qualitatively investigated by the expression of photon flux, i.e. (Eq. (15)). In equation (15), the coefficient $\alpha_0 n_g$ appears twice. The one outside the integral results from the slow light enhanced reemission process, while the second one in the exponential term inside the integral is due to the enhanced reabsorption process of the reemitted light. Hence, for a waveguide with a length of L, there exists an optimum αn_g to realize the maximum retrieval efficiency. In reference [15], there is a conclusion that the maximum retrieval efficiency can be realized under $\alpha_0 L = 2$, in which the impact of the signal bandwidth and the slow light effect in the waveguide are not considered. It can be seen that equation (15) in our result is equivalent with equation (19) in reference [15] if $e^{-\Omega^2/2\Gamma^2}$ and n_g are both replaced by 1, leading to the same conclusion as that in reference [15] under the conditions that the signal bandwidth is extremely narrow and there is no slow light effect in the waveguide.

On the other hand, when the input signal light is the train of N Gaussian pulses mentioned in Section 3, in which the pulses are separated without overlapping, the photon flux of the retrieved pulses can be calculated in the way that equation (15) is obtained, and the result is

$$I_f^{(1)}(L,t) = -\left(\frac{1}{2\pi}\right)^2 (\alpha_0 L n_g)^2 e^{-\left(\frac{2\pi\gamma_a}{\Delta}\right)^2} \times \sum_{j=1}^{N} \left| \int d\Omega e^{i\left[\Omega\left(t - t_{0j} - \frac{2\pi}{\Delta} - \frac{L}{v_g}\right) + \frac{\alpha_0 L n_g n_1(\Omega)}{2}\right]} \times e^{-\frac{\alpha_0 L n_g n_0(\Omega)}{2}} n_0(\Omega)\, a(\Omega) \right|^2, \quad (17)$$

where the trade-off between the enhanced reemission and enhanced reabsorption obviously exists for each pulse. This equation shows that appropriate slow light effect can enhance the retrieval performance of each mode independently in the temporal multimode signal.

By equations (16) and (17), the impact of the slow light effect on the performance of the forward retrieval scheme of the AFC based quantum memory can be analyzed. Figure 3 shows the calculation results.

Figure 3a shows the photon flux I at the input and output ports of the waveguide when the input signal light is a single Gaussian pulse. The waveguide has a low intrinsic absorption depth of $\alpha_0 L = 0.05$. The AFC has a bandwidth of $\Gamma/2\pi = 8$ MHz, a peak-peak spacing $\Delta/2\pi = 1$ MHz, and a single peak width $\gamma_a/2\pi = 0.1$ MHz. The input single Gaussian pulse has a bandwidth of $\gamma_s/2\pi = 3$ MHz. The black dashed line shows the photon flux of the input pulse at the input port, and its center is set as $t = 0$. The red solid and blue dotted lines are the calculated photon fluxes at the output port of the waveguide under $n_g = 2$ and $n_g = 37$, respectively. In the calculation results, the first pulse is the transmitting pulse propagating through the waveguide without interacting with the AFC, which is calculated by equation (8). The second pulse is the retrieved light pulse calculated by equation (16).

It can be seen that the photon flux peak $I_{\max}$ of the transmitting pulse is higher than 0.8 when the $I_{\max}$ of the input pulse is normalized to 1 in the case of $n_g = 2$. On the other hand, the $I_{\max}$ of the retrieved pulse is nearly not visible, since most photons transmits the waveguide without interacting with the AFC. However, the performance of the quantum memory is improved significantly if a moderate slow light effect is introduced with a n_g of 37. The $I_{\max}$ of the transmitting pulse reduces to near 0.02 and that of the retrieved pulse increases to near 0.52, since the slow light effect in the waveguide enhances both the absorption and the reemission processes.

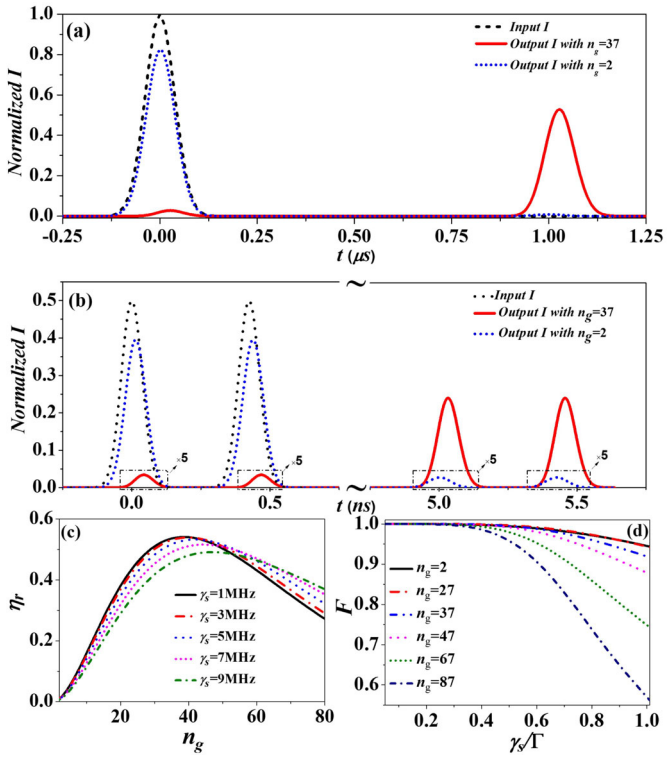

Fig. 3. Calculation results of the performances of the forward retrieval scheme. (a) The stored and retrieved pulses in the forward retrieval scheme when the input light is a single Gaussian pulse. The black dashed line is the normalized photon flux I of the input pulse. The red solid line and the blue dotted line are the normalized photon fluxes I of the output light under $n_g = 37$ and $n_g = 2$, respectively. The AFC parameters are the same to those in Figure 2 and $\gamma_s/2\pi = 3$ MHz. (b) The stored and retrieved pulses in the forward retrieval scheme when the input light is a pulse trains with two Gaussian pulses. The bandwidth of the pulse train is $\gamma_s/2\pi = 3$ GHz. The parameters of the AFC structure are $\Gamma/2\pi = 8$ GHz, $\Delta/2\pi = 200$ MHz, and $\gamma_a/2\pi = 10$ MHz, respectively. (c) The retrieval efficiency η_r of the case shown in (b) under different group index n_g and bandwidth of the pulse train γ_s. (d) The retrieval fidelity F of the case shown in (b) under different n_g and γ_s. Other parameters in (c) and (d) are the same to those in (b).

To show that this scheme can be utilized to store and retrieve the temporal multi-mode signals, Figure 3b shows the calculation result when the input signal light is a pulse train with two Gaussian pulses. In this case, the AFC parameters are set as $\Gamma/2\pi = 8$ GHz, $\Delta/2\pi = 200$ MHz, and $\gamma_a/2\pi = 10$ MHz, respectively. The spectral width of the pulse train is set as $\gamma_s/2\pi = 3$ GHz, and the photon flux peak $I_{\max}$ of each pulse is normalized to be 0.5. These parameters are set to show the feasibility of the storage of the broadband signal in the rare earth doped material with large inhomogeneous broadening [17,26]. The colors and styles of the lines in this figure is the same as those in Figure 3a. It can be seen that the slow light effect in the waveguide can also enhance the performance in this case. The $I_{\max}$ in the retrieved pulse increases to 0.24 under a group index of $n_g = 37$, while the transmitting probability is suppressed significantly.

To show the impact of the slow light effect more clearly, the light retrieval efficiencies η_r in the case shown in Figure 3b are calculated under different group indexes n_g and signal bandwidth γ_s. The results are shown in Figure 3c. It can be seen that at each signal bandwidth, the light retrieval efficiency has a maximum under a specific n_g. It is the result of the tradeoff between the enhancements of the slow light effect on the reemission and reabsorption processes, represented by the terms of $\alpha L n_g$ and $e^{-\alpha L n_g n_0(\Omega)/2}$ in equation (17), respectively. The maximum retrieval efficiency is about 54% at $n_g = 37$ when $\gamma_s/2\pi = 1$ GHz. It reduces with increasing γ_s, while the optimum n_g to realize this maximum increases at the same time. It can be explained by equation (17), in which the optimum n_g to realize the maximum photon flux is different for the components with different frequency detuning Ω. The component with larger Ω requires higher n_g. For a signal with broader bandwidth, the tradeoff should be taken over all the frequency components, leading to a lower peak of retrieval efficiency and a larger optimum n_g to realize it.

According to definition in reference [33], the fidelity of the quantum memory is calculated and the details can be seen in Appendix E of the Supplementary material. Based on this calculation, the fidelity F of the retrieved double pulses shown in Figure 3b is calculated under different n_g and γ_s/Γ and plotted in Figure 3d. It can be seen that F keeps around 100% under arbitrary n_g when the signal bandwidth γ_s is less than 0.3Γ. This means that the slow light effect can simultaneously enhance the storage and retrieval efficiency, and keep the fidelity nearly unit. When γ_s increase under certain n_g, F decreases, and such decrease is more significant under larger n_g. This can be explained by equation (15), in which the frequency-dependent modulation term $e^{i(\alpha_0 L n_g n_1(\Omega)/2)} e^{-\alpha L n_g n_0(\Omega)/2} n_0(\Omega)$ gives larger amplitude and phase differences to different frequency components for signal with larger bandwidth, and the influence of such modulation effect gets stronger monotonously with larger n_g. Although this adverse effect in fidelity is accompanying with slow light, it can be seen in Figure 3d that $n_g = 37$ can still keep the fidelity above 90% even for signal with bandwidth approaching the AFC bandwidth.

4.2 The backward retrieval scheme

As mentioned in Section 2, under two counter- propagating control pulses, light pulses can be backward retrieved. The area of the two control pulses should be π. Though ideal π pulse is impossible to be achieved here due to the inhomogeneous electrical field distribution in PCW, it can be approached by adjusting the temporal width and intensity of the pulses [43]. Neglecting the decoherence and inhomogeneous broadening of the spin coherence in the

AFC, the two control pulses can be treated as being applied simultaneously at time $t = T_0$, defined in the Section 4.1. At $t = T_0$, no backward reemission occurs and the initial value of the backward propagating atomic coherence can be deduced as

$$\hat{\sigma}_b^{ge}(z,T_0;\Omega) = \hat{\sigma}_f^{ge}(z,T_0;\Omega) = \sqrt{2\pi}\kappa\mu_{eg}\int_{-\infty}^{T_0} dt' e^{-i\Omega(T_0-t')}\hat{a}_f(z,t'). \tag{18}$$

Then, similar to equation (2), the dynamic equation of $\hat{\sigma}_b^{ge}(z,t;\Omega)$ can be obtained, and in similar way that equation (13) is deduced, we obtain the equation of the backward propagating field in the PCW as

$$\left(\frac{\partial}{\partial z}-\frac{1}{v_g}\frac{\partial}{\partial z}\right)\hat{a}_f(z,t) = \alpha_0 n_g \times\left[\int_{-\infty}^{T_0} dt'\tilde{n}(t-t')\hat{a}_f(z,t') + \int_{T_0}^{t} dt''\tilde{n}\left(t-t''\right)\hat{a}_b\left(z,t''\right)\right]. \tag{19}$$

In the backward retrieval scheme, the retrieved light backward propagates and outputs from the waveguide at $z = 0$. According to the method used in reference [33], the field operator of the retrieved field is finally obtained as

$$\hat{a}_b^{(1)}(0,t) = -\frac{\alpha_0 n_g}{2\pi}e^{-\frac{\left(\frac{2\pi}{\Delta}\right)^2\gamma_s^2}{2}}\int d\Omega n_0(\Omega) \times\int_0^L dz' e^{i\left(\Omega t-\frac{2\pi}{\Delta}-\frac{2\Omega z'}{v_g}+\alpha_0 n_g n_1(\Omega)z'\right)} \times e^{-\alpha_0 n_g n_0(\Omega)z'}\hat{a}_f(0,\Omega). \tag{20}$$

In the backward retrieval scheme, the remitted wave at the position of z' has a z'-dependent phase shift $2\Omega z'/v_g+\alpha_0 z' n_g n_1(\Omega)$ and amplitude attenuation factor of $e^{-\alpha n_g n_0(\Omega)z'/2}$. Hence, backward propagating waves remitted at different position have different phases and amplitudes. They interfere at $z = 0$ and result in the integral term of $\int_0^L dz' e^{-i2\Omega z'/v_g}e^{\alpha n_g e^{-\Omega^2/2\Gamma^2}z'}$ in equation (20). Such interference is not completely constructive, leading to the phase mismatching phenomenon discussed in reference [33]. Based on equation (20), we can get the photon flux of the retrieved pulse as

$$I_b^{(1)}(0,t) = \langle a_b^{(1)\dagger}(z,t)a_b^{(1)}(z,t)\rangle = \left(\frac{1}{2\pi}\right)^2 e^{-\left(\frac{2\pi}{\Delta}\right)^2\gamma_s^2} \times\int d\Omega_1\int d\Omega_2 F(\Omega_1,\Omega_2 t)\langle a_f^\dagger(0,\Omega_1)\hat{a}_f(0,\Omega_2)\rangle \tag{21a}$$

$$F(\Omega_1,\Omega_2) = e^{i(\Omega_2-\Omega_1)\left(t-\frac{2\pi}{\Delta}\right)}H(\Omega_1)H(\Omega_2)e^{-\frac{\left(\Omega_1^2+\Omega_2^2\right)}{\Gamma^2}} \tag{21b}$$

$$H(\Omega) = \frac{e^{-\alpha n_g n_0(\Omega)L}e^{i\left(-\frac{2\Omega}{v_g}L+\alpha_0 n_g n_1(\Omega)L\right)}-1}{1+i\left(\frac{2\Omega}{\alpha c}-n_1(\Omega)\right)\frac{1}{n_0(\Omega)}} \approx \frac{e^{-\alpha n_g n_0(\Omega)L}e^{i\alpha_0 n_g n_1(\Omega)L}-1}{1-i\frac{n_1(\Omega)}{n_0(\Omega)}}. \tag{21c}$$

In usual experiment of quantum memory, the signal bandwidth is at most tens of GHz, and a typical value of α is 10 cm^{-1}. Hence, $2\Omega/\alpha c$ is much smaller than 1, and the effect of $n_1(\Omega)/n_0(\Omega)$ is dominant, which means the AFC induced dispersion is much stronger than the intrinsic dispersion in waveguide. Therefore, the denominator of $H(\Omega)$ is approximated into $1 - in_1(\Omega)/n_0(\Omega)$ in the last step in equation (21c).

If the single Gaussian pulse input mentioned in Section 4.1 is substituted into equation (21a), a simple expression of $I_b(0,t)$ can be obtained as

$$I_b^{(1)}(0,t) = \left(\frac{1}{2\pi}\right)^2 e^{-\left(\frac{2\pi}{\Delta}\right)^2\gamma_s^2} \times\left|\int d\Omega e^{i\Omega\left(t-\frac{2\pi}{\Delta}\right)}H(\Omega)\alpha(\Omega)\right|^2. \tag{22}$$

We can see that the enhancement of light-atom interaction due to the slow light effect represented by n_g can increase the photon flux of retrieval pulse in an exponential way, even though the reabsorption of the reemitting signal is also enhanced. This effect can be explained by the fact that the interference at $z = 0$ is generated by waves with different amplitudes, which is represented by the term $\int_0^L dz' e^{-\alpha n_g e^{-\Omega^2/2\Gamma^2}z'}$ in equation (20). However, the phase mismatching in such interference leads to the term $in_1(\Omega)/n_0(\Omega)$ in the denominator of $H(\Omega)$ in equation (21c). Since $n_0(\Omega) = e^{-\Omega^2/2\Gamma^2}$ and $n_1(\Omega) = e^{-\Omega^2/2\Gamma^2}\mathrm{erf}i(-\Omega/\sqrt{2}\Gamma)$, $in_1(\Omega)/n_0(\Omega)$ is negligible if the signal bandwidth γ_s is much smaller than AFC bandwidth Γ and equation (22) can be simplified into

$$I_b^{(1)}(0,t) = \left(\frac{1}{2\pi}\right)^2 e^{-\left(\frac{2\pi}{\Delta}\right)^2\gamma_s^2} \times\left|\int d\Omega e^{i\Omega\left(t-\frac{2\pi}{\Delta}\right)}h(\Omega)\alpha(\Omega)\right|^2, \tag{23a}$$

$$h(\Omega) = e^{-\alpha n_g n_0(\Omega)L}e^{i\left(-\frac{2\Omega}{v_g}L+\alpha_0 n_g n_1(\Omega)L\right)}-1. \tag{23b}$$

Equation (23a) is a generalization of equation (A18) in reference [15], in which the signal bandwidth and dispersions are not considered. This expression shows that even though αL is very low, we can realize a high retrieval efficiency close to unit by increasing n_g. However, the result is different at all for the signal light pulse with a bandwidth comparable to Γ, since the term $in_1(\Omega)/n_0(\Omega)$ in equation (21c) cannot be neglected in this case. Similar to equation (22), the photon flux of the retrieval pulse when temporal multi-mode signal is input into the waveguide can be expressed as

$$I_b(0,t) = \left(\frac{1}{2\pi}\right)^2 e^{-\left(\frac{2\pi}{\Delta}\right)^2\gamma_s^2} \times \sum_{j=1}^{N}\left|\int d\Omega e^{i\Omega\left(t-t_{0j}-\frac{2\pi}{\Delta}\right)} H(\Omega)\,\alpha(\Omega)\right|^2. \quad (24)$$

Figure 4 shows the calculation results of the performance of the backward retrieval scheme of the AFC-based quantum memory in PCW with slow light.

In Figure 4a, the output photon flux in the backward scheme is calculated according to equation (24), when the input is a train of two Gaussian pulses with $\gamma_s/2\pi$ = 3 MHz and the AFC parameters are $\Gamma/2\pi$ = 8 MHz, $\Delta/2\pi$ = 1 MHz, and $\gamma_a/2\pi$ = 0.1 MHz, respectively. It can be seen that the normalized photon flux peak of every single pulse in the two retrieved Gaussian pulses is lower than 0.05, and that of every single transmitting pulse is larger than 0.25, when n_g = 2, i.e., nearly no slow light effect exists in the waveguide. Here, the peak photon flux of every pulse in the input two Gaussian pulses is normalized to 0.5. When n_g increases to 37, it can be seen that the peak of every single output pulse is larger than 0.3, while that of the every transmitting pulse is negligible. These results confirm that the storage and retrieval probabilities can be improved significantly with a moderate slow light effect in the waveguide, if the signal light bandwidth is relatively small. In Figure 4b, similar calculations are taken and plotted, while the signal pulses bandwidth are changed to $\gamma_s/2\pi$ = 7 MHz. When n_g = 2, it can be seen that the peak photon flux of the transmitting pulse increases slightly when compared with that in Figure 4a, which is because that the amplitude of the transmitting pulse increases with input signal bandwidth, as shown in Figure 2. Compared with the retrieved pulses under n_g = 2 in Figure 4a, the corresponding pulses in Figure 4b are slightly lower, since the influence of the term $in_1(\Omega)/n_0(\Omega)$ in equation (21c) gets larger when the signal bandwidth increases. The degrade due to the increasing signal bandwidth will be more obvious when n_g increases, since the phase mismatching effect is larger under higher n_g as shown in equation (24). Hence, it can be seen that the peak photon flux of the output pulses under n_g = 37 decreases to lower than 0.2 in Figure 4b. The phase mismatching effect also leads to strong distortion of the retrieved pulses from the input signal pulses, which is more obvious in Figure 4b. It will be particularly discussed below.

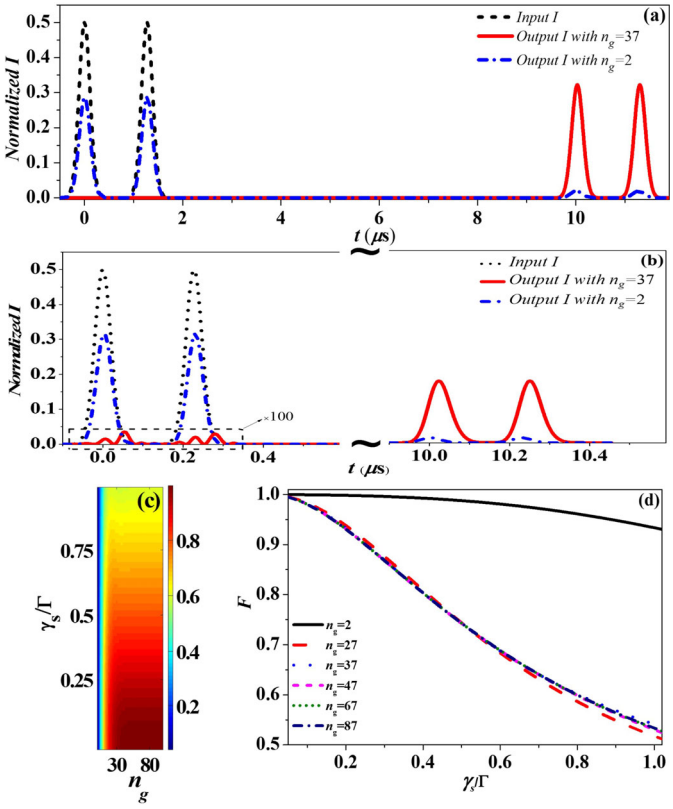

Fig. 4. In the backward retrieval scheme, (a) the photon fluxes I of the stored and retrieved pulses sequence when a train of two Gaussian pulses with a bandwidth of $\gamma_s/2\pi$ = 3 MHz is input into a waveguide with an optical depth of $\alpha_0 L$ = 0.14 and a length of L = 100 μm. The black dashed line is the photon flux I of the input signal. The red solid and blue dashed dot lines present the normalized output photon fluxes with n_g = 37 and n_g = 2, respectively. The parameters of the AFC structure are $\Gamma/2\pi$ = 8 MHz, $\Delta/2\pi$ = 1 MHz, and $\gamma_a/2\pi$ = 0.1 MHz. (b) The same process as (a), but with $\gamma_s/2\pi$ = 7 MHz. The line colors and styles are the same to those in (a). (c) The retrieval efficiency η_r of the process in (a), versus varying γ_s and n_g. (d) The retrieval fidelity F of the process in (a) with increasing γ_s/Γ, when n_g are 2, 27, 37, 47, 67 and 87.

To show the improvement of the slow light effect more clearly, we calculated the retrieval efficiency η_r and showed its dependence on n_g and γ_s/Γ in Figures 4c. In Figure 4c, when γ_s/Γ is smaller than 0.3, η_r can be improved to be above 90% by introducing a moderate n_g of 30∼40. While γ_s/Γ increases, η_r under a fixed n_g deceases significantly, because the phase mismatching effect gets stronger and the interference of the reemitted waves more destructively, i.e., the term $in_1(\Omega)/n_0(\Omega)$ in equation (21c) becomes larger. When γ_s approaches Γ, for example, $\gamma_s = 0.9\Gamma$, even if n_g increases to 80, the retrieval efficiency can only reach 60%. This results show that in the backward retrieval scheme of the AFC-based quantum memory, slow light effect can effectively increases the retrieval efficiency when the bandwidth of the input signal is relatively small, however, the phase mismatching effect

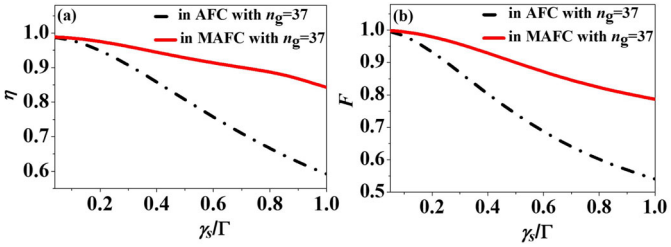

Fig. 5. In the backward retrieval scheme, (a) the retrieval efficiency η versus γ_s/Γ when AFC- (solid) and MAFC-based protocol is employed. (b) The fidelity F versus γ_s/Γ when AFC- (solid) and MAFC-based protocol is employed. In both of (a) and (b), $n_g = 37$ and the parameters of AFC or AFC region in MAFC and signal are same to those in Figure 4d.

limits such improvement in the case that the input signal has a large bandwidth.

The fidelity F of the retrieved signal is also calculated under different γ_s and n_g, which is shown in Figure 4d. It can be seen that F decreases with increasing γ_s for all the n_g since the modulation effect, i.e., the influence of the term $H(\Omega)$ in equation (24) becomes stronger for the signal with large bandwidth γ_s. It is obvious that compared with F without slow light effect, i.e., the case with $n_g = 2$, F with considerable slow light effect is much lower, and the $F-\gamma_s$ curves for $n_g = 27$, 37, 47, 67 and 87 are nearly the same with each other. It can be also explained by that the constructive extent of the interference in retrieval process becomes weaker with an increasing n_g, which leads to more differences on the responses for different frequency components Ω. However, it can be seen in Figure 4d that for input signal γ_s smaller than $\Gamma/4$, the fidelity F can keep higher than 90%.

Figures 4c and 4d reveal that the phase mismatching limits the improvement of retrieval efficiency and brings fidelity falling for signal with broadband signal in slowing light enhanced quantum memory based on backward retrieval AFC protocol. In reference [33], modified atomic frequency comb (MAFC) is proposed to cancel the dispersion in atomic ensemble. Here, if MAFC is prepared in PCW with low intrinsic optical depth, phase mismatching can be suppressed, and therefore the improvements on retrieval efficiency and fidelity can be achieved simultaneously in the slowing light enhancement, for broadband signal.

In Figures 5a and 5b, the retrieval efficiency and fidelity dependence on γ_s/Γ in both of normal AFC and MAFC are calculated and plotted, respectively. The detailed structure of MAFC can be seen in Appendix E of the Supplementary material, and the calculation is based on replacing the AFC induced dispersion term $e^{i(\alpha_0 n_g n_1(\Omega)z/2)}$ by MAFC induced dispersion term. In Figure 5a, for signal with bandwidth of $\gamma_s = 0.8\Gamma$, slow light with $n_g = 37$ can increase the retrieval efficiency η to larger than 90% and keep the fidelity F above 82% in MAFC-based protocol, while the same slow light can only give η lower than 60% and fidelity lower than 55% in MAFC-based protocol.

5 Discussion on the physical implement

When PCW is introduced into quantum memory, several special properties of PCW should be considered. Firstly, the dispersion would distort the signal in storage and retrieval processes. Hence, PCW with low dispersions in their slow light regime are preferred in this scheme. In recent years, several such slow light photonic crystal waveguide designs have been proposed and demonstrated [38,39], which are promising in this application. Secondly, in the quantum memory in PCW, the light coupling efficiency of the slow light mode is also important for the total retrieval efficiency. Although there might be large mode field mismatching between the slow light mode in PCW and the mode of output waveguide [37], various designs on the coupling region of the slow light PCW have been proposed and very high coupling efficiencies have been demonstrated [44–46], which can be used to improve the retrieval efficiency of the memory. Moreover, propagation loss in the PCW is also a crucial issue in our scheme since large loss will reduce the storage and retrieval efficiency significantly. However, thanks to the developed fabrication technology and special design on photonic crystal, the typical loss in PCW can be easily controlled to be lower than 100 dB/cm [47,48]. Our calculation in Section 4 shows that a PCW length of 100 μm is long enough to achieve strong enhancement on quantum memory, and the propagation loss in such waveguide is acceptable.

As mentioned in the introduction, most experiments of the AFC quantum memory are implemented in bulk crystals doped by rare earth ions. Recently, some on-chip realizations of the AFC quantum memory have been reported using optical waveguide structures on the doped crystals [26,27]. The slow light effect could be introduced in the waveguides on the chips of doped crystals by fabricating photonic crystal (PC) structures on them. Many works have been done on the fabrication of PC and PC waveguides on the $LiNbO_3$ wafers [49,50], aiming at their applications in nonlinear optical devices. On the other hand, recently the nano-beam structure with 1D PC structure has been successfully fabricated on a Nd-doped Y_2SiO_5 crystal, which is another kind of crystal used as a quantum interface between light and rare earth ions [51].

Slow light structures and microcavities are two important structures to enhance the on-chip interaction between light and matters. They have some differences in enhancing the AFC-based quantum memory. Firstly, in the scheme based on microcavities, the AFC dispersion would narrow the linewidth of the cavity mode [31,32], which reduces the retrieval efficiency and fidelity of the storage of a broadband signal. While, the broadband signal can be stored and retrieved effectively in the scheme based on PCWs with low dispersion according to the calculations in Section 4, since the limitation of the resonance linewidth does not exist. Secondly, the measurement of the prepared AFC in the cavity is difficult due to the interaction between the AFC and the cavity mode [31]. Hence, in reference [31] the measurement is realized by destroying the cavity structure. The scheme based on slow light PCWs does not have this problem. Moreover, as shown

in Figure 4c, the retrieval efficiency of a narrowband signal can approach unit by slow light enhancement if the PCW is short enough and the propagation loss is negligible. While, the efficiency would be much lower than unit in a microcavity due to its unavoidable intrinsic loss.

Based on the calculations in Figure 4 and above discussions, we can expect a typical physical implement of our scheme. Based on the PCW made of Pr^{3+}:Y_2SiO_5 crystals, if the AFC bandwidth is 5 MHz and a temporal multimode signal with a bandwidth of 2 MHz input into the slow light mode with $n_g = 37$, a retrieval efficiency higher than 50% and a fidelity larger than 90% can be achieved in forward retrieval scheme. If backward retrieval scheme is adopted and MAFC is designed, the retrieval efficiency will be higher than 95% with a fidelity higher than 90%. In recent years, several designs of slow light PCWs with large n_g were proposed and demonstrated [38–40], showing that the developed micro- and nanofabrication technology can support the realization of the PCW with a n_g of 30∼40 over a sufficient bandwidth for the application of AFC based quantum memory. Therefore, the moderate n_g around 37 in a broad bandwidth, utilized in the calculation, is realizable by the current technologies.

6 Conclusions

In this paper, we propose a high efficiency AFC quantum memory scheme based on rare earth ion doped waveguide with slow light. Its performance was investigated theoretically. Both the forward and backward retrieval schemes of AFC based quantum memory were analyzed, by introducing the slow group velocity into the coupled evolution equations of the atomic ensemble and the electromagnetic field with considerable bandwidth. In the forward retrieval scheme, a moderate slow light effect can increase the retrieval efficiency to a value higher than 50%, for both the narrowband signal and the signal with a bandwidth approaching the AFC bandwidth Γ, while high fidelity can be kept. In the backward retrieval scheme, a moderate n_g can increase the retrieval efficiency to be larger than 95% and keep the fidelity higher than 90% for signal with bandwidth much narrower than Γ. For signal with bandwidth approaching Γ, such improvement is limited by the phase mismatching effect, which is overcome by introducing the MAFC. The calculation results show that although the effects of the slow light effect is quite complicated in this AFC-based quantum memory, overall it is positive, providing a promising way to realize high efficiency on-chip quantum memory.

This work was supported by 973 Programs of China under Contract Nos. 2013CB328700 and 2011CBA00303, National Natural Science Foundation of China (61575102 and 61321004), Basic Research Foundation of Tsinghua National Laboratory for Information Science and Technology (TNList).

References

1. H.J. Kimble, Nature (London) **453**, 1023 (2008)
2. N. Sangouard, C. Simon, H. de Riedmatten, N. Gisin, Rev. Mod. Phys. **83**, 33 (2011)
3. L.M. Duan, M.D. Lukin, J.I. Cirac, P. Zoller, Nature (London) **414**, 413 (2001)
4. T. Chanelière, D.N. Matsukevich, S.D. Jenkins, S.-Y. Lan, T.A.B. Kennedy, A. Kuzmich, Nature (London) **438**, 833 (2005)
5. S. Abruzzo, H. Kampermann, D. Bruß, Phys. Rev. A **89**, 012301 (2014)
6. J.J. Longdell, E. Fraval, M.J. Sellars, N.B. Manson, Phys. Rev. Lett. **95**, 063601 (2005)
7. G. Heinze, C. Hubrich, T. Halfmann, Phys. Rev. Lett. **111**, 033601 (2013)
8. K.F. Reim, P. Michelberger, K.C. Lee, J. Nunn, N.K. Langford, I.A. Walmsley, Phys. Rev. Lett. **107**, 053603 (2011)
9. D.S. Ding, W. Zhang, Z.Y. Zhou, S. Shi, B.S. Shi, G.C. Guo, Nat. Photon. **9**, 332 (2015)
10. S.A. Moiseev, S. Kröll, Phys. Rev. Lett. **87**, 173601 (2001)
11. A.L. Alexander, J.J. Longdell, M.J. Sellars, N.B. Manson, Phys. Rev. Lett. **96**, 043602 (2006)
12. M.P. Hedges, J.J. Longdell, Y.M. Li, M.J. Sellars, Nature (London) **465**, 1052 (2010)
13. V. Damon, M. Bonarota, A. Louchet-Chauvet, T. Chanelière, J.-L. Le Gouët, New J. Phys. **13**, 093031 (2011)
14. J. Dajczgewand, J.-L. Le Gouët, A. Louchet-Chauvet, T. Chanelière, Opt. Lett. **39**, 2711 (2014)
15. M. Afzelius, C. Simon, H. de Riedmatten, N. Gisin, Phys. Rev. A **79**, 052329 (2009)
16. H. de Riedmatten, M. Afzelius, M.U. Staudt, C. Simon, N. Gisin, Nature (London) **456**, 773 (2008)
17. E. Saglamyurek, J. Jin, V.B. Verma, M.D. Shaw, F. Marsili, S.W. Nam, D. Oblak, W. Tittel, Nat. Photon. **9**, 83 (2015)
18. C. Clausen, I. Usmani, F. Bussières, N. Sangouard, M. Afzelius, H. de Riedmatten, N. Gisin, Nature (London) **469**, 508 (2011)
19. Z.Q. Zhou, W.B. Lin, M. Yang, C.F. Li, G.C. Guo, Phys. Rev. Lett. **108**, 190505 (2012)
20. M. Gündoğan, P.M. Ledingham, A. Almasi, M. Cristiani, H. de Riedmatten, Phys. Rev. Lett. **108**, 190504 (2012)
21. A. Tiranov, J. Lavoie, A. Ferrier, P. Goldner, V.B. Verma, S.W. Nam, R.P. Mirin, A.E. Lita, F. Marsili, H. Herrmann, C. Silberhorn, N. Gisin, M. Afzelius, F. Bussières, Optica **2**, 279 (2015)
22. M. Gündoğan, P.M. Ledingham, K. Kutluer, M. Mazzera, H. de Riedmatten, Phys. Rev. Lett. **114**, 230501 (2015)
23. M. Lovriæ, D. Suter, A. Ferrier, P. Goldner, Phys. Rev. Lett. **111**, 020503 (2013)
24. M. Hosseini, B.M. Sparkes, G. Campbell, P.K. Lam, B.C. Buchler, Nat. Commun. **2**, 174 (2011)
25. N.B. Phillips, A.V. Gorshkov, I. Novikova, Phys. Rev. A **78**, 023801 (2008)
26. E. Saglamyurek, N. Sinclair, J. Jin, J.A. Slater, D. Oblak, F. Bussières, M. George, R. Ricken, W. Sohler, W. Tittel, Nature (London) **469**, 512 (2011)
27. E. Saglamyurek, N. Sinclair, J. Jin, J.A. Slater, D. Oblak, F. Bussières, M. George, R. Ricken, W. Sohler, W. Tittel, Phys. Rev. Lett. **108**, 083602 (2012)

28. A. Amari, A. Walther, M. Sabooni, M. Huang, S. Kröll, M. Afzelius, I. Usmani, B. Lauritzen, N. Sangouard, H. de Riedmatten, N. Gisin, J. Lumin. **130**, 1579 (2010)
29. M. Afzelius, C. Simon, Phys. Rev. A **82**, 022310 (2010)
30. S.A. Moiseev, S.N. Andrianov, F.F. Gubaidullin, Phys. Rev. A **82**, 022311 (2010)
31. M. Sabooni, Q. Li, S. Kröll, L. Rippe, Phys. Rev. Lett. **110**, 133604 (2013)
32. M. Sabooni, S.T. Kometa, A. Thuresson, S. Kröll, L. Rippe, New J. Phys. **15**, 035025 (2013)
33. S. A Moiseev, J.-L. Le Gouët, J. Phys. B **45**, 124003 (2012)
34. S.A. Moiseev, M.I. Noskov, Laser Phys. Lett. **1**, 303 (2004)
35. S.A. Moiseev, B.S. Ham, Phys. Rev. A **70**, 063809 (2004)
36. S.A. Moiseev, Bull. Russ. Acad. Sci. Phys. **68**, 1408 (2004)
37. T.F. Krauss, J. Phys. D **40**, 2666 (2007)
38. S. Kubo, D. Mori, T. Baba, Opt. Lett. **32**, 2981 (2007)
39. Y. Hamachi, S. Kubo, T. Baba, Opt. Lett. **34**, 1072 (2009)
40. R. Geiss, S. Diziain, R. Iliew, C. Etrich, H. Hartung, N. Janunts, F. Schrempel, F. Lederer, T. Pertsch, E.B. Kley, Appl. Phys. Lett. **97**, 131109 (2010)
41. F.L. Kien, S.D. Gupta, V.I. Balykin, K. Hakuta, Phys. Rev. A **72**, 032509 (2005)
42. F.L. Kien, K. Hakuta, Phys. Rev. A **79**, 013818 (2009)
43. S. Marzban, J.G. Bartholomew, S. Madden, K. Vu, M.J. Sellars, Phys. Rev. Lett **115**, 013601 (2015)
44. J.P. Hugonin, P. Lalanne, T.P. White, T.F. Krauss, Opt. Lett. **32**, 2638 (2009)
45. Y.A. Vlasov, S.J. McNab, Opt. Lett. **31**, 50 (2009)
46. C.Y. Lin, X. Wang, S. Chakravarty, B.S. Lee, W.-C. Lai, R.T. Chen, Appl. Phys. Lett. **97**, 183302 (2010)
47. E. Kuramochi, M. Notomi, S. Hughes, A. Shinya, T. Watanabe, L. Ramunno, Phys. Rev. B **72**, 161318 (2005)
48. M. Settle, M. Salib, A. Michaeli, T.F. Krauss, Opt. Express **14**, 2440 (2006)
49. N. Courjal, J. Dahdah, G. Ulliac, P. Sevillano, B. Guichardaz, F. Baida, Opt. Express **19**, 23008 (2011)
50. F. Sulser, G. Poberaj, M. Koechlin, P. Günter, Opt. Express **17**, 20291 (2011)
51. T. Zhong, J. Kindem, E. Miyazono, A. Faraon, Nat. Commun. **6**, 8206 (2015)